SAND2022-3688C

Proceedings of the ASME 2022 Pressure Vessels & Piping Conference
ASME/PVP 2022
July 17–22, 2022, Las Vegas, NV, USA

PVP2022-83904

FATIGUE DESIGN SENSITIVITIES OF STATIONARY TYPE 2 HIGH-PRESSURE HYDROGEN VESSELS

John M. Emery*
Materials and Failure Modeling Department
Sandia National Laboratories
Albuquerque, NM 87123
Email: jmemery@sandia.gov

Peter Grimmer
Solid Mechanics Department
Sandia National Laboratories
Albuquerque, NM 87123

Robert Wheeler III
Chris San Marchi
Joseph Ronevich
Hydrogen and Materials Science Department
Sandia National Laboratories
Livermore, CA 94550

ABSTRACT

Type 2 high-pressure hydrogen vessels for storage at hydrogen refueling stations are designed assuming a predefined operational pressure cycle and targeted autofrettage conditions. However, the resulting finite life depends significantly on variables associated with the autofrettage process and the pressure cycles actually realized during service, which many times are not to the full range of the design. Clear guidance for cycle counting is lacking, therefore industry often defaults to counting every repressurization as a full range pressure cycle, which is an overly conservative approach. In-service pressure cycles used to predict the growth of cracks in operational pressure vessels results in significantly longer life, since most in-service pressure cycles are only a fraction of the full design pressure range. Fatigue crack growth rates can vary widely for a given pressure range depending on the details of the residual strains imparted during the autofrettage process because of their influence on crack driving forces. Small changes in variables associated with the autofrettage process, e.g., the target autofrettage overburden pressure, can result in large changes in the residual stress profile leading to possibly degraded fatigue life.

In this paper, computational simulation was used for sensitivity studies to evaluate the effect of both operating conditions and autofrettage conditions on fatigue life for Type 2 high-pressure hydrogen vessels. The analysis in this paper explores these sensitivities, and the results are used to provide guidance on cycle counting. In particular, we identify the pressure cycle ranges that can be ignored over the life of the vessel as having negligible effect on fatigue life. This study also examines the sensitivity of design life to the autofrettage process and the impact on life if the targeted residual strain is not achieved during manufacturing.

INTRODUCTION

In this paper, fatigue life of a high-pressure, carbon-fiber overwrapped, steel liner hydrogen storage tank is explored through computational simulation. The calculations considered a longitudinal crack in the liner steel. The objective of these calculations was to probe sensitivities to the many design, material and environmental parameters that contribute to finite fatigue life. Here, Abaqus [1] and FRANC3D [2] were used for crack growth simulation in the presence of residual stress to establish a look-up table for crack driving force versus crack length. Subsequently, crack growth rate data for steel in gaseous hydrogen was used [3] to estimate fatigue life. The calculations considered a longitudinal crack in the wall of an idealized autofrettaged vessel whose dimensions, liner and overwrap inner and outer diameters, were take from representative industry design.

A baseline analysis is first established considering the maximum operating conditions and conservative crack growth rate data published prior to the release of Code Case 2938. From this, a threshold pressure cycle that leads to negligible fatigue crack

*Address all correspondence to this author.

growth is computed and used to simply but conservatively evaluate in-service pressure cycling data previously reported in [4]. It is expected, of course, that this type of philosophy be thoroughly vetted by the community prior to adoption of such a method.

Following this, deviation from the baseline fatigue life caused by off-design residual stress is considered. Here, the autofrettage simulation is modified by a relatively small change in the autofrettage overburden pressure, which results in a significant reduction in the compressive residual stress, and the crack growth calculations are repeated. The outcome demonstrates one source of possible design uncertainty and loss of margin.

The remainder of this paper is organized as follows. The following section describes the computational approach used to simulate fatigue life of the autofrettaged pressure vessel for the baseline scenario. The subsequent section introduces variations in the analyses to explore design sensitivities. Then, a discussion section is presented that summarizes observations from the sensitivity exploration. This is followed by the conclusions section.

COMPUTATIONAL METHODS

In this section the computational methods used to estimate fatigue life are described using the nominal design parameters throughout. The focus of the analyses was on a type II high-pressure, carbon-fiber overwrapped hydrogen storage tank. The first step in the analysis process involves solving for the residual stress field imparted during the autofrettage process. This requires a nonlinear finite-element (FE) calculation that simulates the manufacturing process. After estimating the residual stress field, linear elastic fracture mechanics (LEFM) was used to simulate the fatigue crack growth, superposing the stress fields resulting from the operating pressures and the residual stress fields. This series of calculations establishes the relationship between crack depth, a, and the mode-one stress intensity factor K_I. Finally, data describing the fatigue crack growth rate versus the driving force is used to estimate fatigue life.

Autofrettage simulation

To estimate the residual stress field resulting from the autofrettage process, a FE model of the pressure vessel, including the liner and overwrap, was developed and is shown in Figure 1. In the figure, the liner appears red and the overwrap appears cyan, and nominal dimensions are listed. Boundary conditions were applied so that the vessel was simply supported and free to expand with internal pressurization. An isotropic, elasto-plastic model was used to represent the SA-372 Grade J Class 70 liner steel and the hardening behavior was taken from tensile tests performed in both axial and circumferential directions conducted at Sandia. (There was no evidence to suggest the material behaved anisotropically.) Table 1 lists relevant materials properties that describe the liner steel including the elastic modulus, the yield strength σ_{yield}, the ultimate strength σ_u, and the ductility ε_u. We assumed the carbon fiber overwrap material was isotropic and remained elastic with Young's modulus of 68 GPa. The consideration of overwrap anisotropy is left to future work. The materials are assumed to be rate and temperature independent.

TABLE 1. Line material properties.

Modulus (GPa)	σ_{yield} (MPa)	σ_u (MPa)	ε_u (%)
206	762	995	27

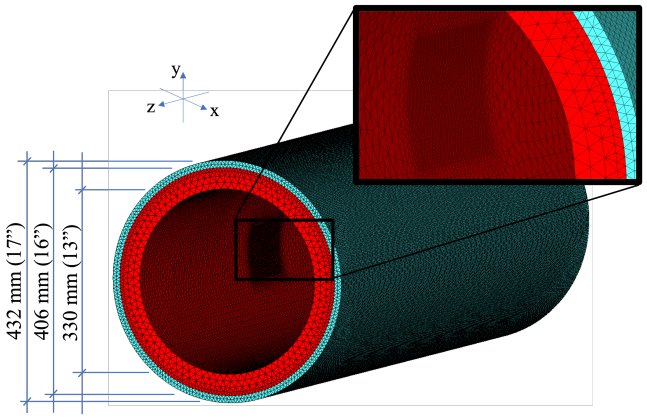

FIGURE 1. Schematic of the FE model and mesh showing nominal pressure vessel dimensions and mesh refinement in the region of crack propagation.

There is uncertainty in the autofrettage process, but the simulation targeted hoop strain of 0.5% on the external fibers of the overwrap, which was achieved with an autofrettage pressure of 230 MPa. Kinematic boundary conditions were implemented so that internal pressure was the only cause of deformation, while maintaining global stability. Figure 2 shows the estimated compressive residual stress field (minimum principal stress contour), which was greatest in magnitude on the inside of the tank at approximately 300 MPa. The Abaqus C3D10 general purpose tetrahedral element formulation was used [1], and mesh convergence was explored with one-level of mesh coarsening and the fields presented here represent a converged solution for residual stress.

Crack growth simulation

Crack growth simulation was performed using the fracture mechanics code FRANC3D [2]. FRANC3D is a pre- and post-processing code that modifies a FE input database to include the

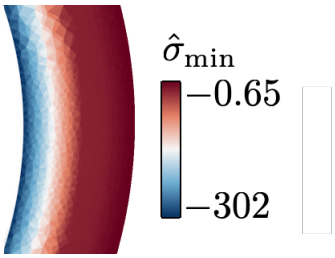

FIGURE 2. Minimum principal stress contour plot showing the residual stress field resulting from the autofrettage process (stress units: MPa).

geometry and mesh of a crack, calls the FE solution engine, and post-processes the FE output database. The post-processing step computes the crack driving forces based on the FE solution, estimates the new crack geometry, and updates the FE mesh for the predicted crack growth. For the analysis here, the materials were assumed to be elastic, and the crack growth was assumed to be sub-critical and governed by small-scale yielding so that LEFM applies. Hence, this process is not conducted for every fatigue cycle, as it would be cost prohibitive and unnecessary. Rather, the goal is to establish the relationship between the crack geometry and attendant driving forces. This relationship can be conceptualized as the following function that is dependent on crack length a and tank pressure P,

$$\mathrm{K_I}(\mathrm{P}, a) = \mathrm{K_I^P}(\mathrm{P}, a) + \mathrm{K_{I,auto}}(a) \tag{1}$$

where $\mathrm{K_I^P}$ is the driving force caused by the internal pressure, and $\mathrm{K_{I,auto}}$ is the result of the residual stress due to the autofrettage process, which is independent of the tank pressure. $\mathrm{K_{I,auto}}$ is negative when the residual stress is compressive.

The analysis here considers a longitudinal crack originating on the inside wall of the pressure vessel, initially 500 µm deep and with a depth-to-surface length aspect ratio of 1/3, $\frac{a}{2c} = 1/3$. Crack growth at each crack-front mesh node was dictated by the difference between the positive driving force resulting from pressurization of the tank to its maximum operating pressure of 93.1 MPa and the negative driving forced caused by the compressive residual stress. Increments of crack growth at each crack-front mesh node were user-defined and chosen to be proportional to crack growth rate data in gaseous hydrogen environments collected by co-authors [3] and summarized in the ASME BPVC Code Case 2938, Table 1 [5]. The fracture toughness of this steel was measured in hydrogen to be approximately 50 MPa$\sqrt{\mathrm{m}}$. Figure 3 shows the shape of predicted crack growth. Each solid black line corresponds with the crack front for a user-specified increment of crack growth, and the spacing between the crack fronts lines is not indicative of rate. The general trend is for faster crack growth at the deeper point of the crack because the compressive residual stress is greater near the inner wall of the vessel. This is consistent with experimental observations found in the literature [6].

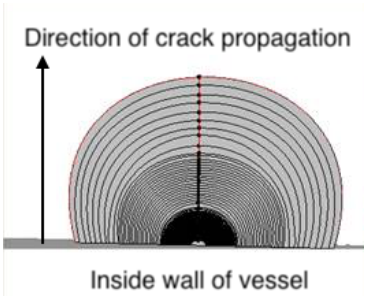

FIGURE 3. The predicted crack shape, showing slowed crack growth on the inside wall of the vessel where compressive residual stresses are highest.

Figure 4 plots mode-one stress intensity factor $\mathrm{K_I}$ versus the crack depth normalized by the liner wall thickness. The blue curve is the mode-one stress intensity factor corresponding to the maximum operating pressure. The red curve corresponds to the residual stress that would otherwise force the crack closed (interpenetrating). The orange curve is the sum of these two and represents the stress intensity factor at maximum operating pressure. For the maximum operating pressure of 93.1 MPa, and an initial crack depth of 0.5 mm, $\mathrm{K_I^P}$ = 12.3 MPa$\sqrt{\mathrm{m}}$, $\mathrm{K_{I,auto}}$ = -9.5 MPa$\sqrt{\mathrm{m}}$, and their sum is $\mathrm{K_I}$ = 2.8 MPa$\sqrt{\mathrm{m}}$. This curve is subsequently used as a look-up table for driving force in fatigue life estimates. A convenience of the application of LEFM is that, for cycle pressures lower than the maximum operating pressure, $\mathrm{K_I^P}$ is computed by a linear scaling of the blue curve by the ratio of the appropriate pressures.

Fatigue life calculation

Fatigue life is dictated by the range in crack driving force $\Delta\mathrm{K}$ and stress intensity factor ratio $\mathrm{R_K}$,

$$\Delta\mathrm{K} = \mathrm{K_{I,max}} - \mathrm{K_{I,min}} \tag{2}$$

$$\mathrm{R_K} = \mathrm{K_{I,min}}/\mathrm{K_{I,max}} \tag{3}$$

where by Eq. (1) $\mathrm{K_{I,max}} = \mathrm{K_I^P}(\mathrm{P_{max}}, a) + \mathrm{K_{I,auto}}(a)$ is the stress intensity factor corresponding with the maximum pressure $\mathrm{P_{max}}$ and $\mathrm{K_{I,min}} = \mathrm{K_I^P}(\mathrm{P_{min}}, a) + \mathrm{K_{I,auto}}(a)$ is the stress intensity factor corresponding with the minimum pressure $\mathrm{P_{min}}$ in the loading cycle N. Evidently, the negative residual stresses introduced by the autofrettage process have no effect on the range of the crack

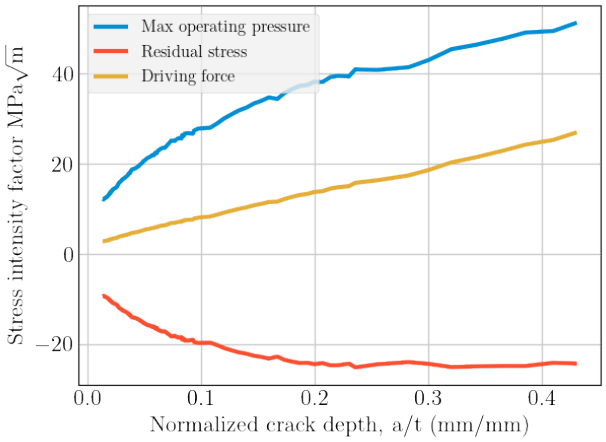

FIGURE 4. Crack driving force versus normalized crack depth for the maximum operating pressure (blue), the residual stress (red), and their sum (orange, labeled "driving force").

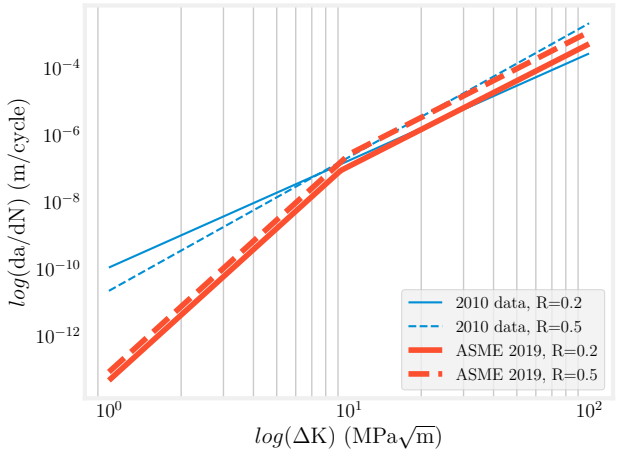

FIGURE 5. Crack growth rate curves for two loading ratios, R = 0.2 and 0.5, for SA-372 Grade J steel per ASME BPVC Code Case 2938, Table 1M (labeled ASME 2019) and previous 2010 data (labeled 2010 data).

driving force,

$$\begin{aligned}\Delta K &= K_I^P(P_{max},a) + K_{I,auto}(a) - (K_I^P(P_{min},a) + K_{I,auto}(a)) \\ &= K_I^P(P_{max},a) - K_I^P(P_{min},a)\end{aligned}$$

but they do influence the loading ratio,

$$R_K = \frac{K_I^P(P_{min},a) + K_{I,auto}(a)}{K_I^P(P_{max},a) + K_{I,auto}(a)} \neq \frac{K_I^P(P_{min},a)}{K_I^P(P_{max},a)}.$$

Prior to formalization of design curves by the approval of ASME BPVC Code Case 2938 in December of 2018, fatigue crack growth rate data were published circa 2010 which were used for a design basis; however, the data was over a limited ΔK range and resulted in an overly-conservative design. Data for crack growth rate is typically reported for various loading ratios in logarithmic plots of rate crack growth rate versus stress intensity factor range. Figure 5 plots best-fit curves from circa 2010 data and design curves from Code Case 2938 for load ratios of 0.2 and 0.5. The Code Case 2938 design curves corresponded to data in lower ΔK ranges, and shows considerably lower rates than extrapolated data. For stress intensity ranges near 1 MPa$\sqrt{\text{m}}$ there is over two orders of magnitude difference. Code Case 2938 offers a formula for the resulting bi-linear crack growth rate relationship. Interestingly, the different load ratio curves for the older data cross each other, showing inverse behavior at decreasing load ratio. This plays a role in the following analysis.

The fatigue analysis in this section uses the crack growth rate from the earlier 2010 data and the relationship between driving force and crack length established in Figure 4. The assumed operation of the tank was 5,040 full operating pressure cycles, 93.1 MPa to 61.4 MPa, with two full blowdown cycles, 93.1 MPa to 0.0 MPa per year. These operating conditions were extracted from original design considerations and are summarized in Table 2. With these parameters, the crack growth rate was integrated to a final crack depth equal to 25% of the liner wall thickness and the estimated fatigue life was 36.9 years, or 185,700 cycles. The estimated evolution of the crack depth is shown in Figure 6.

TABLE 2. Assumed maximum operating conditions for the hydrogen refueling tank.

cycles/year	Max pressure (MPa)	ΔP (MPa)	Load ratio $R_P = \frac{P_{min}}{P_{max}}$
5,040	93.1	31.7	0.66
2	93.1	93.1	0.

SENSITIVITY

In this section, we explore the sensitivity of the fatigue prediction to several factors.

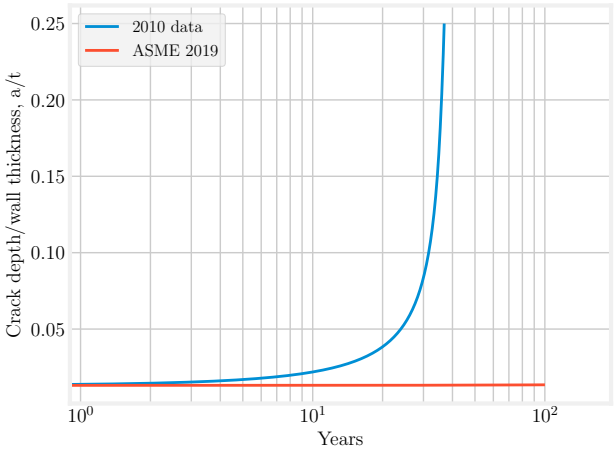

FIGURE 6. Estimated crack depth versus time for 5,040 maximum operating pressure cycles plus two full blowdown cycles per year based on the 2010 crack growth rate data.

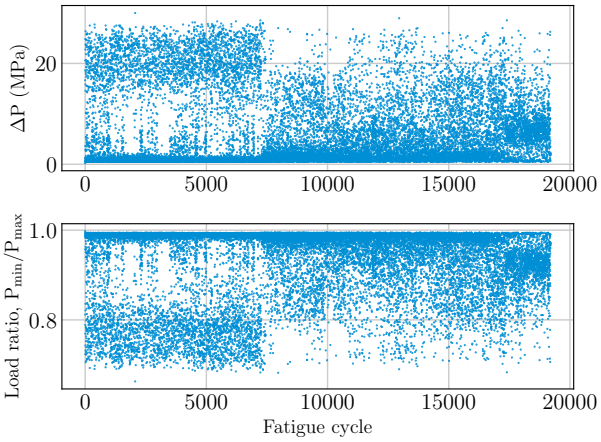

FIGURE 7. Pressure range and pressure ratio for usage data from an in-service refueling tank.

In-service pressure cycles

Data previously presented by coauthors [4] from in-service pressure cycling suggests, at least for one refueling station, there are many fluctuations that are well below the maximum design pressure cycle. A sample of such data is provided in Figure 7. The data spans approximately three years of service with 19,257 pressure fluctuations and 2 full blowdown cycles. The median pressure range is 3.6 MPa and the first quartile pressure range is 1.0 MPa. However, without clear guidance, these less severe pressure cycle ranges are counted as full cycles against the fatigue life. This motivates a desire to identify a threshold pressure cycle, at or below which negligible crack growth is expected, so that these cycles could be neglected. Since the driving force is proportional to the square root of crack length, the pressure threshold will change as the crack grows and the tank ages.

To establish such a relationship, we first identify the driving force range that corresponds with threshold growth, ΔKth. Let $\frac{da}{dN} = f(\Delta K; R)$ define a function f describing the crack growth rate, plotted in Figure 5, dependent on ΔK and R. We would like to find $\Delta K = g(\frac{da}{dN}; R)$, the inverse function $g = f^{-1}$ and solve for $\Delta Kth = g(\frac{da}{dN}_{th}; R)$ with $R \in [-1, 1]$. Here we use $\frac{da}{dN}_{th} = 0.1\,\text{nm/cycle}$. (From ASTM E647: For most materials an operational, though arbitrary, definition of ΔKth is given as that ΔKth which corresponds to a fatigue crack growth rate of $0.1\,\text{nm/cycle}$.) Figure 8 shows the relationship between ΔKth and non-negative loading ratio R for both the current ASME crack growth guidance (labeled ASME 2019) and 2010 data (labeled 2010 data). Note, the ΔKth increases for the older guidance due to the crossing of the crack growth rate curves previously pointed out. Further note, ΔKth of approximately 3.4 $\text{MPa}\sqrt{\text{m}}$ for $R_K = 0$ by the ASME 2019 curves, is considerably above the estimate of $K_I = 2.8\ \text{MPa}\sqrt{\text{m}}$ for an initial 0.5 mm deep crack.

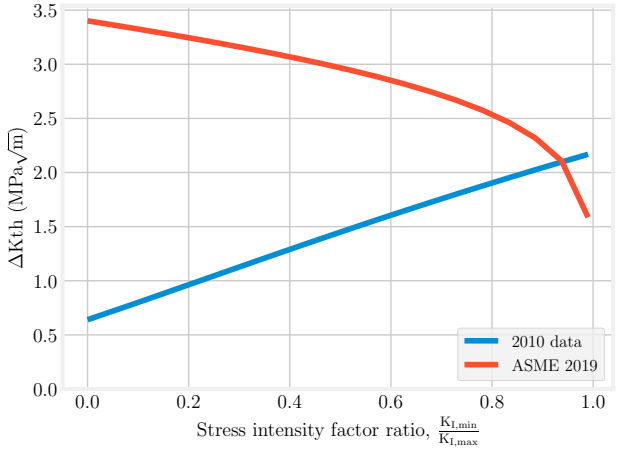

FIGURE 8. Threshold stress intensity factor range ΔKth versus loading ratio $R_K \geq 0$ for crack growth rate data from both ASME 2010 and 2019 code case.

For autofrettaged vessels, compressive residual stress has the effect of imposing a negative driving force. From Eq. (1), when $K_I(P, a) + K_{I,auto} < 0$, *e.g.* for small cracks or for the minimum load in a pressure cycle range, the driving force is non-physical (interpenetration). If such is the case when computing $K_{I,min}$, design guidance in Code Case 2938 indicates that the driving force for the minimum load be set to 0 in all equations, and hence by Eq. (2) $\Delta K = K_{I,max}$ and by Eq (3) $R_K = 0$. This was implemented with the following Python function:

```
def computeDK(dp,a,R_p,Kp,Kauto):
    ''' Compute the \Delta K range

    Parameters
    ----------
    dp : <float> pressure cycle range, Pmax - Pmin
    a : <float> crack length
    R_p : <float> loading ratio, Pmin/Pmax
    Kp : <callable> function taking crack pressure
        and crack length to evaluate the driving
        force
    Kauto : <callable> function taking % of
        autofrettage pressure and crack length to
        evaluate the effects of residual stress

    Return:
    -------
    [dki, R_K] : [<float>, <float>] the \Delta K
        range and load ratio defined by Kmin/Kmax
        Note: R_K != R_P::
            R_K = {(Kmin+Kauto) > 0.,
                   (Kmin+Kauto)/(Kmax+Kauto), 0.}
            R_P = Pmin/Pmax
    '''
    pmax=dp/(1-R_p)
    pmin=pmax-dp
    kmax=Kp(pmax,a)
    kmin=Kp(pmin,a)
    kauto=Kauto(1.,a)
    R_K=(kmin+kauto)/(kmax+kauto)
    #
    if kmin + kauto < 0.:
        kmin = 0.
        R_K = 0.0
        kmax+=kauto
    #
    dki=kmax-kmin
    if dki < 0.: dki = 0.

    return [dki, R_K]
```

The outcome of implementing this guidance is plotted in Figure 9 for the two pressure cycles occurring in the maximum operating conditions presented in Table 2. The top axis plots the fatigue crack driving force, while the bottom axis plots the stress intensity factor ratio. For smaller cracks up to about a/t = 0.155, the stress intensity factor range is equivalent for both pressure ratios and dictated by $K_{I,max} = K_I^P(P_{max}, a) + K_{I,auto}(a)$. The stress intensity factor ratio is also impacted and remains zero up to this point. Afterwards, the stress intensity factor ratio is dictated by Eq. (3) and will differ from the pressure ratio. Noting from Figure 8 that ΔK_{th} is approximately 0.6 MPa$\sqrt{m}$ for $R_P = 0$ and increases to approximately 1.6 MPa$\sqrt{m}$ for $R_P = 0.66$, it appears there are no negligible crack growth cycles for the maximum operating conditions using the 2010 crack growth rate data. However, by the same observations, it appears there is predicted to be *no crack growth* per the 2019 CC2938 guidance.

With ΔK_{th} and the crack driving force per crack length established, corresponding pressure range ΔP_{th} can be computed as a function of crack length using the relationship established in Figure 4. Following, the crack length can be related to the age of the pressure vessel based on the relationship plotted in Figure 6. Figure 10 plots the resulting relationship between threshold pressure cycle range and vessel age in years, but the story does not end here.

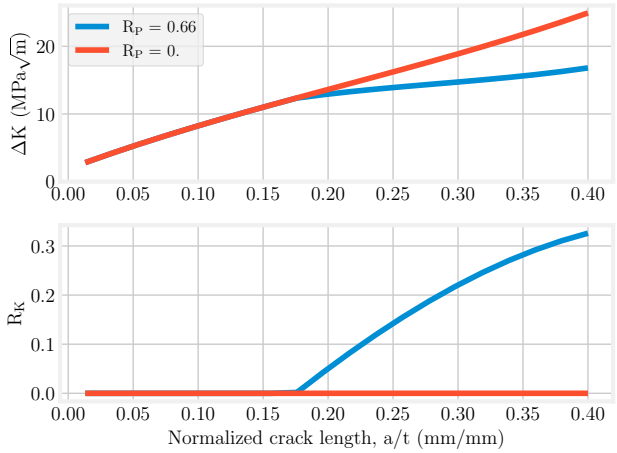

FIGURE 9. Fatigue crack driving force (top) and stress intensity factor ratio (bottom) versus normalized crack depth for load ratios of R_P=0 and R_P=0.66.

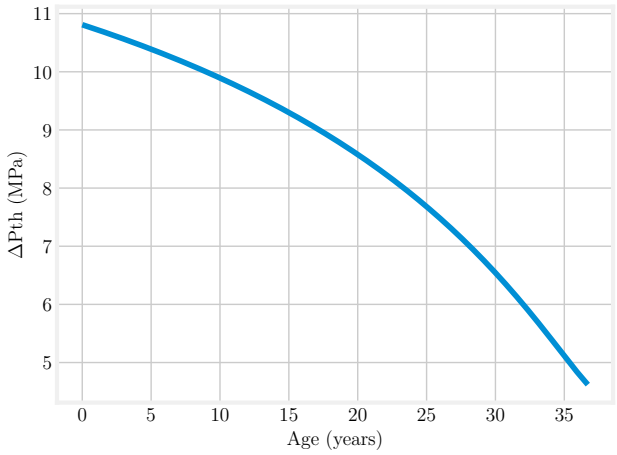

FIGURE 10. Pressure cycle threshold versus tank age in years for crack growth rate data from the 2010 data assuming the maximum operating conditions described in Table 2, *i.e.*, P_{max} = 93.1 MPa.

Using the pressure cycle threshold, a simplified fatigue eval-

uation can be created for managing a refueling station based on actual tank usage. The proposed simplified evaluation appears below in Algorithm 1. In this algorithm, an effective tank age N_{eff} is maintained based on pressure cycles above the threshold and is used to evaluate the current threshold based on Figure 10 and crack length based on Figure 6. The outcome is shown in Figure 11 where crack depth is plotted versus tank age. In addition to the estimate from the simplified algorithm, the figure includes the estimate for the maximum operating conditions, and the estimate based on explicitly integrating the tank data from Figure 7 repetitively until $a/t = 0.25$. The degree of conservatism in the current design stands out immediately when comparing the maximum operation curve against the estimate based on in-service data. The simplified analysis is seen to significantly extend the estimated fatigue life of the vessel, while remaining conservative.

Data: a, N, N_{eff}
Result: Fatigue life estimate
initialization;
$a = 0.5$; N=$N_{eff} = 0$;
while $a/t \leq 0.25$ **do**
  $\Delta P \leftarrow next$; N+=1;
  eval $\Delta P_{th}(N_{eff})$;
  if $\Delta P \geq \Delta P_{th}$ **then**
    $N_{eff} += 1$;
    $a = a(N_{eff})$;
  end
  if $N == N_{final}$ **then**
    STOP
  end
end

Algorithm 1: Simplified fatigue life evaluation.

Residual stress

The estimated fatigue life is strongly dependent on the residual stress field imparted during the autofrettage process. To inspect these sensitivities, the autofrettage simulation was modified to use 90% of the autofrettage pressure for a final pressure of 0.9*230 = 207 MPa. This reduction led to a final compressive stress on the inside of the vessel of approximately 182 MPa, which is approximately a 61% reduction. Figure 12 plots the stress intensity factors for the maximum operating pressure, the residual stress field, and their sum for both the full autofrettage pressure (solid lines) and the 90% reduction (dashed lines). Spline interpolation was used in this figure to smooth the data from the crack growth simulations. The curves differ considerably both in magnitude and shape. Perhaps surprisingly, there

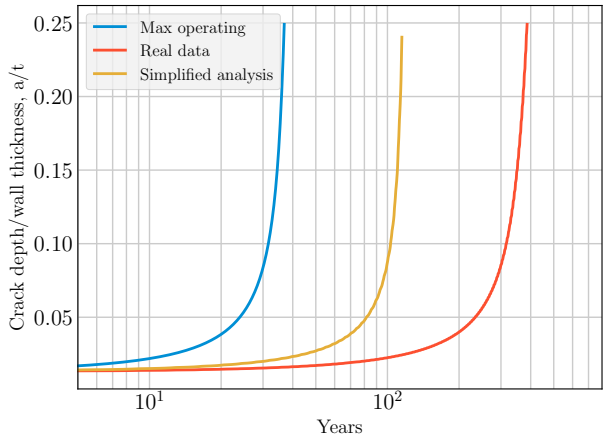

FIGURE 11. Crack depth versus time estimated for maximum operating conditions (blue), in-service data (red), and a simplified analysis (orange).

was a predicted difference in the stress intensity factor caused by the maximum operating pressure, particularly above $a/t = 0.2$. This was caused by greater crack growth at the surface for the reduced residual stress case, ultimately amounting to greater crack area and thus a higher driving force.

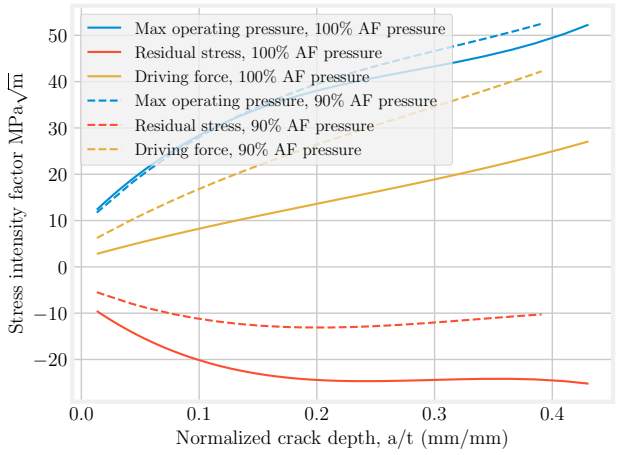

FIGURE 12. Crack driving force for the full autofrettage process (solid lines) and 90% of the autofrettage pressure (dashed lines).

Fatigue life estimates for the maximum operating conditions were made for various levels of reduced compressive residual stress. To achieve stress states between 100% and 61%, linear interpolation between the available stress intensity factor solu-

tions was used. This analysis was conducted for both the 2010 data and the 2019 ASME crack growth rate guidance and for various initial flaw sizes. The results are plotted in Figures 13 and 14. The fatigue life assessment was truncated at 20 years for all scenarios, which is manifest in the figures as a horizontal line at 20 years for most curves.

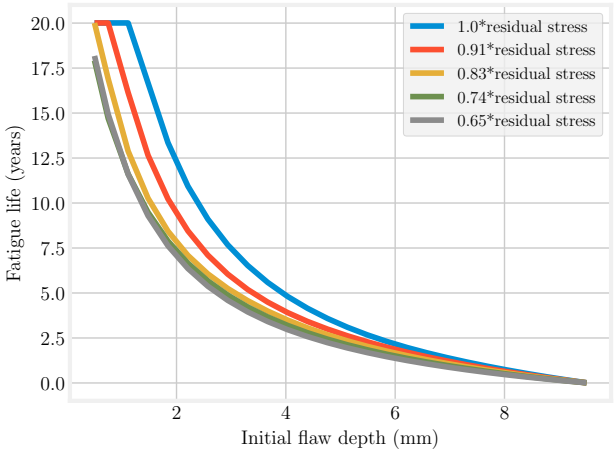

FIGURE 13. The impact on fatigue life of various reductions in residual stress for a range of initial flaw sizes based on the 2010 crack growth rate data.

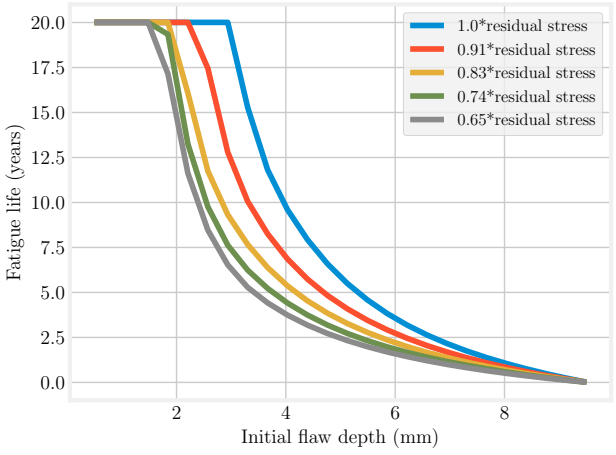

FIGURE 14. The impact on fatigue life of various reductions in residual stress for a range of initial flaw sizes based on the ASME 2019 crack growth rate guidance.

Data in this form could be used as guidance for non-destructive evaluation (NDE) to inform inspection interval based on a perceived confidence in the autofrettage process. For example, for the 2010 data in Figure 13, if the smallest detectable flaw is on the order of 1 mm and it is assumed that 75% of the desired residual stress was achieved, inspection would be encouraged within the first 10 years of tank life.

DISCUSSION

Crack growth rate data from the current Code Case 2938 shows much of the analyses here to be quite conservative due to the orders of magnitude difference for low ΔK ranges. This is apparent from the estimate of fatigue life for the maximum design operation presented in Figure 6. Indeed, comparing ΔK_{th} for the 2019 guidance plotted in Figure 8 versus the driving forces plotted in Figure 4, it seems evident that small initial cracks will, for intents and purposes, remain stationary.

This story, however, changes when one considers reduced residual stress as plotted in Figure 12. The manufacturing process has fairly tight process controls, so it it may be unlikely to miss the desired autofrettage pressure by 10%. However, the residual stresses produced are also strongly dependent on the plastic evolution of the liner steel. While not reported herein, it has been observed that small changes in the yield strength or hardening modulus of the steel can lead to significant changes in the residual stress. These combination of possibilities and the observations with regards to in-service data led to the development of the simplified fatigue estimation Algorithm 1. With a tool like this, fuel station vendors can account for cycles realized, allowing them to extend the life of their pressure vessels while still demonstrating appropriate conservatism.

CONCLUSIONS

In summary, we used computational simulation to explore the conditions leading to fatigue-governed design life of Type 2 high-pressure hydrogen storage vessels used in refueling stations. The autofrettage process was simulated and crack growth calculations were performed in the presence of the resulting residual stress fields. With these, crack growth rate curves were used to estimate the fatigue life of the pressure vessel per baseline maximum operating conditions. Subsequently, sensitivity to in-service pressure cycle data, residual stress fields, and differing guidance in crack growth rate was explored.

The important results included:

- A threshold pressure cycle range was determined.
- The threshold pressure cycle was used with a simplified fatigue estimation algorithm that remained conservative.
- Sensitivity to residual stress fields were demonstrated to significantly impact margin.

ACKNOWLEDGMENT

Sandia National Laboratories is a multimission laboratory managed and operated by National Technology and Engineering Solutions of Sandia, LLC., a wholly owned subsidiary of Honeywell International, Inc., for the U.S. Department of Energy's National Nuclear Security Administration under contract DE-NA-0003525. This work is supported by the U.S. Department of Energy, through the Office of Energy Efficiency and Renewable Energy's (EERE) Hydrogen and Fuel Cell Technologies Office (HFTO). This paper describes objective technical results and analysis. Any subjective views or opinions that might be expressed in the paper do not necessarily represent the views of the U.S. Department of Energy or the United States Government.

REFERENCES

[1] *ABAQUS/Standard User's Manual, v6.14*. Dassault Systèmes Simulia Corp, United States.

[2] *FRANC3D Reference Manual, Version 8.0*. Fracture Analysis Consultants, Inc., United States, Dec 2021.

[3] San Marchi, C., Ronevich, J., Bortot, P., Wada, Y., Felbaum, J., and Rana, M., 2019. "Technical basis for master curve for fatigue crack growth of ferritic steels in high-pressure gaseous hydrogen in asme section viii-3 code". In Pressure Vessels and Piping Conference, Vol. 58929, American Society of Mechanical Engineers, p. V001T01A044.

[4] Ronevich, J. A., San Marchi, C., Brooks, D., Emery, J. M., Grimmer, P., Chant, E., Sims, J. R., Belokobylka, A., Farese, D., and Felbaum, J., 2021. "Exploring life extension opportunities of high-pressure hydrogen pressure vessels at refueling stations". In Pressure Vessels and Piping Conference, Vol. 85338, American Society of Mechanical Engineers, p. V003T05A011.

[5] *ASME Boiler and Pressure Vessel Code: An International Code*. American Society of Mechanical Engineers New York, 2019.

[6] Wada, Y., and Yanagisawa, Y., 2017. "Fatigue crack growth behavior of autofrettaged hydrogen pressure vessel made of low alloy steel". In Pressure Vessels and Piping Conference, Vol. 58004, American Society of Mechanical Engineers, p. V06BT06A043.